WPJET1-PR(17) 17885

P Batistoni et al.

Calibration of JET Neutron Detectors

Preprint of Paper to be submitted for publication in
Review of Scientific Instruments

This work has been carried out within the framework of the EUROfusion Consortium and has received funding from the Euratom research and training programme 2014-2018 under grant agreement No 633053. The views and opinions expressed herein do not necessarily reflect those of the European Commission.

CALIBRATION OF JET NEUTRON DETECTORS

Paola Batistoni[a], S. Popovichev[b], S. Conroy[c], I. Lengar[d], A. Čufar[d], M. Abhangi[e], L. Snoj[d] L. Horton[f] and JET contributors[1]

[a]ENEA, Department of Fusion and Technology for Nuclear Safety and Security, I-00044 Frascati (Rome), Italy
[b]CCFE, Culham Science Centre, Abingdon, Oxon, OX14 3DB, UK
[c]Department of Physics and Astronomy, Uppsala University, Sweden
[d]Reactor Physics Division, Jo˘zef Stefan Institute, Jamova cesta 39, SI-1000 Ljubljana, Slovenia
[e]Institute for Plasma Research, Bhat, Gandhinagar-382428, Gujarat, India
[f]JET Exploitation Unit, Culham Science Centre, Abingdon, Oxon, OX14 3DB, UK

** Corresponding author: paola.batistoni@enea.it*

Abstract

The present paper describes the findings of the calibration of JET neutron yield monitors performed in 2013 using a ^{252}Cf source deployed inside the JET torus by the remote handling system, with particular regard to the calibration of fission chambers (KN1) which provide the time resolved neutron yield from JET plasmas. The experimental data obtained in toroidal, radial and vertical scans are presented. These data are first analysed following an analytical approach adopted in the previous neutron calibrations at JET. In this way, a calibration function for the volumetric plasma source is derived which allows to understand the importance of the different plasma regions and of different spatial profiles of neutron emissivity on KN1 response. Neutronics analyses have also been performed to calculate the correction factors needed to derive the plasma calibration factors taking into account the different energy spectrum and angular emission distribution of the calibrating (point) ^{252}Cf source, the discrete positions compared to the plasma volumetric source, and the calibration circumstances. All correction factors are presented and discussed. We discuss also the lessons learnt which are the basis for the on-going 14 MeV neutron calibration at JET and for ITER.

1. Introduction

An accurate knowledge of the neutron yield is required in fusion reactors to derive the fusion power and other plasma parameters, as well as of the Tritium burnt in fusion reactions, which must be known for Tritium accountancy. It is also required to evaluate the activation and radiation damage of irradiated materials, the resultant radiation loads to sensitive components, and the biological dose rate distributions. Several types of neutron detectors are usually employed which need to be absolutely calibrated in order to provide a measurement of the fusion power. In ITER, the required accuracy for neutron yield measurements is ±10% over the whole range of neutron emission rate, ranging from 10^{14} n/s (in Deuterium

[1] *Overview of the JET results in support to ITER* by X. Litaudon et al. to be published in Nuclear Fusion Special issue: overview and summary reports from the 26th Fusion Energy Conference (Kyoto, Japan, 17-22 October 2016)

operations, producing 2.5 MeV neutrons) up to almost 10^{21} n/s (in Deuterium-Tritium operations, producing 14 MeV neutrons). Achieving such accuracy is challenging in fusion devices because of the size of the plasma neutron source, and because of the size and complexity of the reactor itself. The usual procedure adopted so far in fusion devices to calibrate neutron detectors is based on recording neutron detector signals when a calibrating neutron source of known intensity is deployed inside the machine at different toroidal and poloidal locations.

JET, the largest operating fusion device, like ITER employs both active detectors located around the machine (^{235}U, ^{238}U fission chambers) to monitor the time evolution of the neutron emission rate, and an activation system which pneumatically delivers and retrieves capsules to/from locations inside the torus to the edge of the vacuum vessel. Capsules are delivered before and retrieved after the plasma pulse for counting of the induced gamma radioactivity. The fission chamber (FC) neutron monitors comprise 3 pairs of moderated ion chambers containing ^{235}U and ^{238}U respectively, mounted in moderator packages at locations midway up the transformer magnet limbs in Octants 2, 6 and 8. These are (for ^{235}U) insensitive to neutron energy and cover the neutron emission rate range from 10^{10} to 10^{18} neutrons per second. They were calibrated directly with respect to a standardized ^{252}Cf fission source inside the torus vessel in 1984/9. Accuracies of ± 8% -10 % have been achieved [1, 2, 3, 4].

A significant change in the calibration value was noted already between 1984 and 1989 due to the installation of several new large systems in the torus hall outside the JET vacuum vessel. As these changes in calibration conditions continued, the internal activation system has been used to carry forward the absolute calibration and to cross-calibrate the fission chambers in plasmas with particular conditions. The sensitivity of the activation system is unaltered by changes in the devices outside the vacuum vessel. Changes made inside the vessel have a small effect and have historically been treated by calculated corrections. In 2011, however, the ITER-like Wall has been installed with Be, Be-coated, W and W-coated tiles replacing the CFC tiles previously used [5]. These major changes required a new calibration which has been carried out in 2013, based on the use of a ^{252}Cf spontaneous fission neutron source with intensity 2.62×10^{8} n/s deployed inside the vacuum vessel by means of the JET remote handling (RH) boom [6]. For the activation system calibration data an almost complete analysis was presented in [6], indicating about 15% lower activation coefficients than those previously used and which led to a correspondingly 15% higher JET neutron yields after reprocessing.

The present paper describes the findings of the 2013 calibrations with particular regard to the FC measurements, which were not presented in [6]. The experimental data obtained in the different circumstances have been analysed. Neutronics analyses have also been performed to calculate the correction factors needed to derive the plasma calibration factors taking into account the different energy spectrum of the calibrating (point) ^{252}Cf source, its anisotropic angular emission distribution due to shielding effect of the source capsule and baton, and the discrete positions compared to the plasma volumetric source. We discuss also the lessons learnt which are the basis for the on-going 14 MeV neutron calibration at JET and for ITER. A new calibration at 14 MeV neutron energy is now needed to allow accurate measurements of the fusion power and of plasma ion parameters as a new Deuterium-Tritium campaign is planned at JET in 2019 [7].

2. Fission Chambers Measurements

In order to calibrate the fission chambers, the ^{252}Cf source was positioned at about 200 different poloidal and toroidal positions to simulate the extended plasma source. The source was inserted inside the vessel by the RH boom through the Octant 5 main horizontal port (Fig.1 left). The selected 40 toroidal source positions (Fig.1 right) were along the plasma toroidal axis (central ring, located at R=300 cm, Z=30 cm, C), and along other four rings radially and vertically (Basket Scan, see sketch in Fig. 2 left) displaced around the central one, centred at R=250 cm, Z=30 cm (inner ring, I), R=350, Z=30 cm (outer ring, O), R=300, Z=80 cm (upper ring, U), R=300, Z=-20 cm (lower ring, L), respectively, to investigate the effect of plasma centre displacement and profile variations on the calibration factors. The uncertainty in positioning the neutron source was estimated to be ±2cm by the RH team.

The central ring was repeated to establish the reproducibility of measurements. Checks on the effect of the presence of the RH boom included firstly the 'Overlap' measurements where the points around Octant 1 were measured with clockwise (left) and anticlockwise (right) boom approach and, secondly, measurements near Octant 5 where the boom enters the vessel. These were done with the boom withdrawn into the Octant 5 port and the mascot arms just protruding into the vessel (the 'no boom' position) as well as with the boom curled up in the vessel (when neutron scattering was worsened). During the experiment, 1000 s counting periods were used with the three FC's counting simultaneously.

Port scans were also carried out at Octants 7 and 8 with the source displaced from central positions (31 and 37, respectively) by -75, -50, -25, +25, +50, +75 cm both vertically and radially (see sketch in Fig. 2 left). The data obtained allowed an understanding of the importance of the different plasma regions and of different spatial profiles of neutron emissivity. The JET horizontal ports are centred at Z=0 and extend vertically from about Z=-60 cm to Z=60 cm.

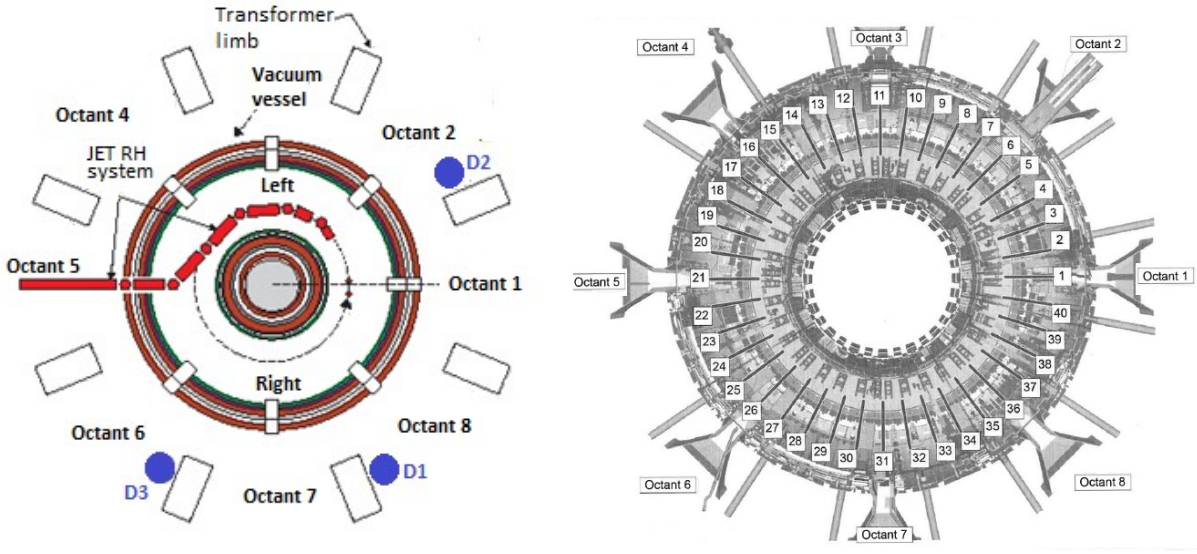

Fig.1 *Sketch showing the position of the D1, D2 and D3 fission chambers and the RH boom deployment inside the JET torus (left). Neutron source positions for ring scan patterns in the JET torus (right)*

The central ring data is summarised for all three detectors in Fig. 3, which also includes the Octant 8 port scan and the counts obtained during the KN2 measurements. Note that no corrections have been applied to these data, apart from subtraction of the random backgrounds in the FCs and renormalisation of the extended counting times for the activation system measurements to 1000 s. After the background subtraction, the total counts integrated over the central ring were 25510, 14695 and 29207 for D1, D2 and D3, respectively (the background amounted to 1%, 6% and 5% respectively). The shapes of each detector response vary due to the different configuration of the closest ports. The response function of the detector in Octant 2 is significantly lower than for the other detectors, due to the presence of the ITER-like Antenna in the Octant 2 main horizontal port. The response peak for the Octant 6 detector is much narrower because the angular view of the line of sight is reduced by two limiters closely set to the port.

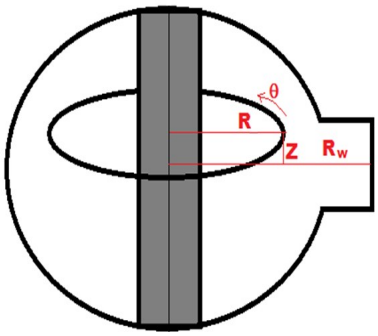

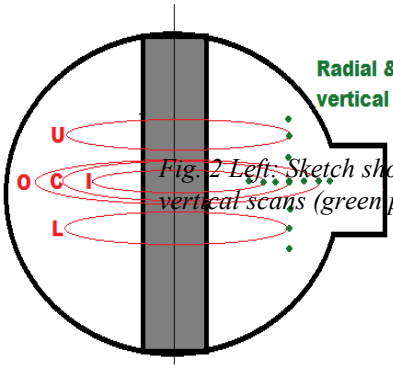

Fig. 2 Left: Sketch showing the 'Basket Scan' rings (red) and the port radial and vertical scans (green points). Right: the parameters R_j, Z_j defining a ring and the radius R_w of the scattering centre

$$S_{Ring}(R,Z,\gamma)=S_0\left\{1-\left[(R-300)^2+(Z-30)^2\right]\right\}^{\gamma}$$

The central ring data and repeat data (Basket Scan central ring) for all three detectors are given in Fig. 4, showing the high reproducibility of the measurements: the integral of the rings data differ less than 1 % in all cases. The five-ring 'Basket Scan' data are shown in Figs 5. The data show that the central scan data agree well with the lower position data. This is because the lower and central rings are just 20 cm below and 30 cm above the port central height which determines the neutron escape probability. The upper ring is less favoured than the lower because it is 50 cm further vertically upwards from the port centre. In the port region, the outer ring is more favoured as it is nearer to the port while the more distant inner ring is relatively disadvantaged. However, the inner ring has a wider peak due to a toroidally-prolonged line of sight advantage for port escape of neutrons.

Moving from the central to the inner and the outer rings caused a maximum change in the integral responses of fission chambers of -7.3% and +9.9% respectively. Moving from the central ring to the upper

and the lower rings caused a maximum change in the integral responses of fission chambers of -11% and -3.6%, respectively, the reduction being mainly due to the increased collimating effect of the vessel main horizontal ports (see Table 1).

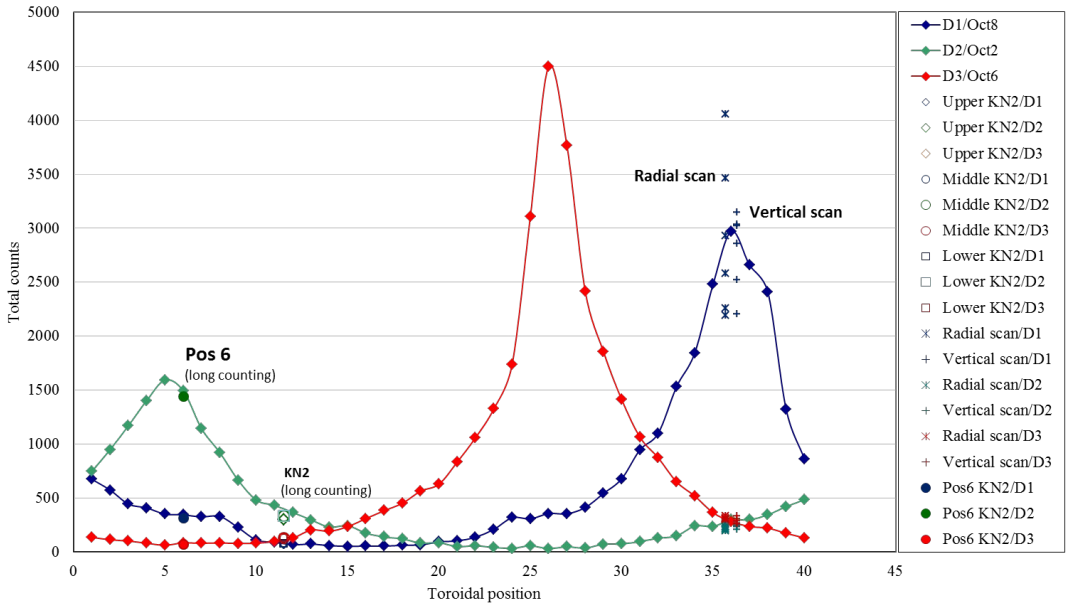

Fig. 3 *Fission chambers central ring data for all three detectors, octant 8 scan and data from long counts during activation irradiations.*

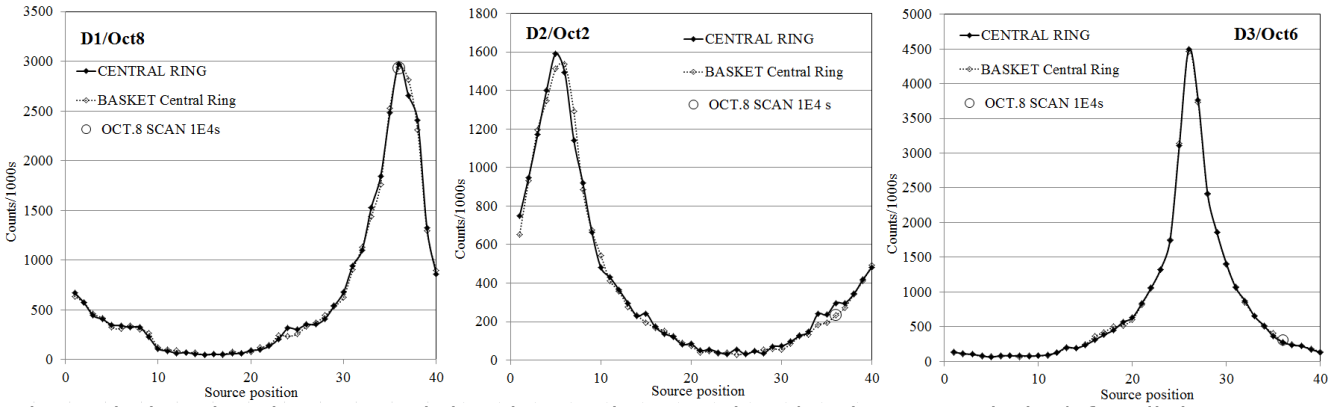

Fig. 4 *Fission chambers central ring data and repeat data (Basket Central Ring) for all three detectors*

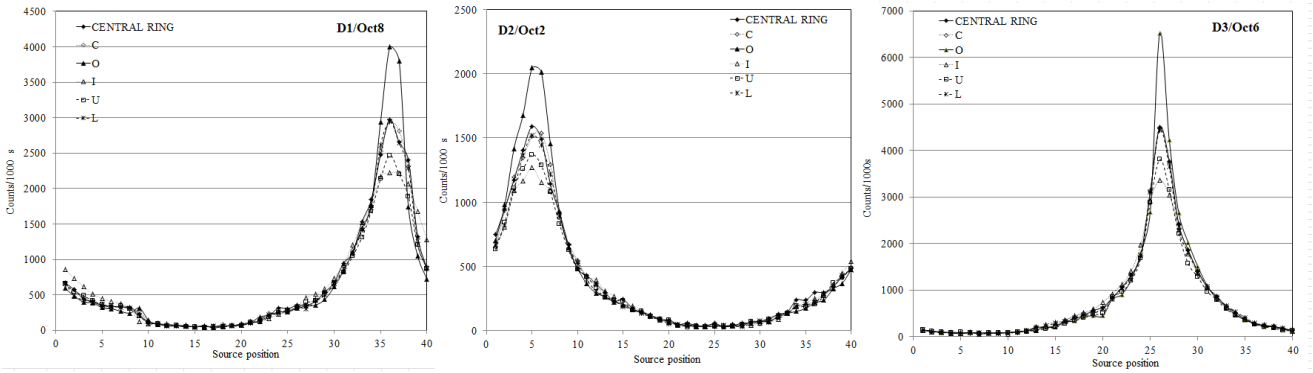

Fig.5 *Basket scan data (C=Central, U=Upper, L=Lower, I= Inner, O=Outer) and central ring data for the three fission chambers*

Table 1 *Integrals of the FCs counts over the 40 toroidal positions for the Basket Scan rings normalized to the integral for the central ring*

	Central Ring	Upper Ring	Lower Ring	Inner Ring	Outer Ring
D1 / Octant 8	1	0.90	0.98	1.00	1.04
D2 / Octant 2	1	0.92	0.96	0.92	1.10
D3 / Octant 6	1	0.89	0.99	0.95	1.06

The results of 'Overlap' measurements around Octant 1 are shown in Fig.6 and compared with the central ring data (for which positions 1-3 where obtained with left approach and 39-40 with right approach). The error bars represent the statistical uncertainty in the measurements. The data show that when the boom body is fully in front of the port and impedes the streaming of neutrons through it (positions 3 from right and 39 from left), the response of closest detectors in Octants 2 and 8 is reduced, indicating the importance of neutrons escaping through the open port. The case of Octant 6 is different as in the central ring the boom body in positions 39 and 40 has a right approach and shields neutrons emitted towards the detector in Octant 6. In this case, the effect of presence of the boom for these particular positions amounts to about 20%. In addition to the statistical uncertainty on the measurements, however, the uncertainty on the positioning of the neutron source has to be taken into account (±2 cm).

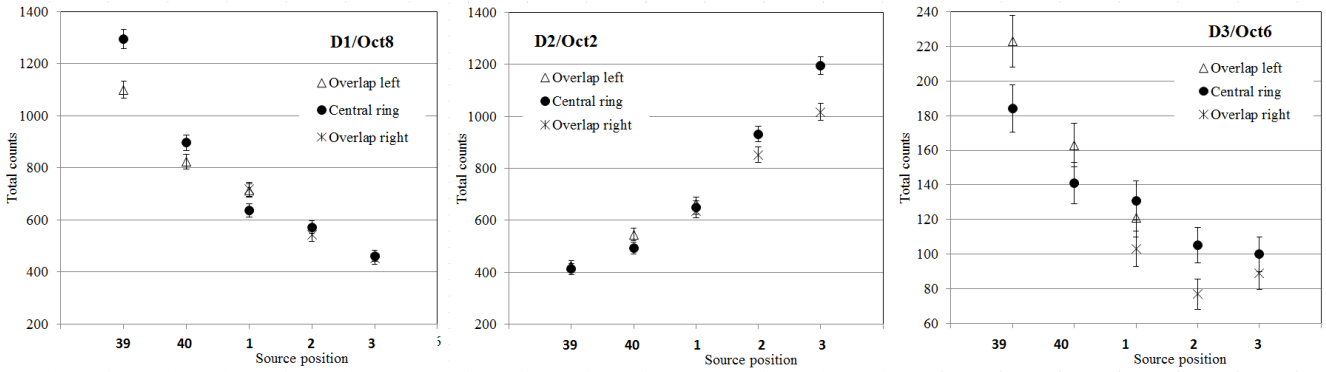

Fig.6 *Overlap data around Octant 1 and central ring data for the three fission chambers*

3. Analysis of KN1 data

In the present paper, it is proposed to generalise the calibration procedure of O.N. Jarvis et al. [2], primarily by extending the analysis to the present situation in

which the normal centre of neutron emission is above the vessel mid-plane (at Z_0=30 cm). One begins with the same assumption that the measured signal is dominated by neutrons scattered from the nearest port into the fission chamber and writes:

$$C_{point}(R,\theta,Z;R_w)=\frac{S_{point}\cdot F(R,\theta,Z)\cdot P}{4\pi ¿¿} \quad (0)$$

where S_{point} is the neutron source intensity (n/s), R_w is the radius of the scattering centre at the port window in the octant where the detector is located, $X^2=¿$ is the square of the distance between the point of emission and the port scattering centre, P is the probability of a neutron reaching the port being detected and $F(R,\theta,Z)$ is the screening factor of the JET structure.
On the assumption that the screening factor is weakly dependent on R for scans done directly in front of the port ($\theta=0$) and at constant height ($Z=30\,cm$), one can derive the effective scattering radius from the radial scan data. Figure 7(left) shows the variation of $C_{point}\cdot X^2$ for the radial scan for $R_w=618\,cm$ which gives values of $C_{point}\cdot X^2$ that are approximately constant across the scan. This value of R_w is larger than the port flange radius of $568\,cm$, indicating that scattering from large ex-vessel objects has increased importance compare to 1980s. This also means that R_w may now vary from port-to-port and thus detector-to-detector.

Varying the effective scattering radius in order to obtain invariance of $C_{point}\cdot X^2$ across the vertical scan data leads to a smaller value of $R_{w,v}=470\,cmR_w=470\,cm$ (Fig.7 right). This is similar to the results in [2], in which R_w is taken as the port flange position of $568\,cm$ for a radial scan and found to be $464\,cm$ for a vertical scan. The smaller value for the vertical scan is thought to be related to the increased importance of scattering from the port walls as the source is moved away from the port centreline and the area of the port flange directly exposed to the source is decreased.

Expanding the angular dependence of $F(R,\theta,Z)$ as a series of cosine functions:

$$F(R,\theta,Z)=F_0(R,Z)\sum_i a_i\cos[(i-1)\theta] \quad (0)$$

with $\sum_i a_i=1$ gives:

$$C_{point}(R,\theta,Z)=\frac{S_{point}P\,F_0(R,Z)}{4\pi}\frac{\sum_i a_i\cos[(i-1)\theta]}{¿¿} \quad (0)$$

The peak count rate, $C_{point,0}$, for a point source of strength S directly in front of the port at $\theta=0$ can be used to normalize the response:

$$C_{point,0}(R,Z)=\frac{S_{point}P\,F_0(R,Z)}{4\pi[(R_w-R)^2+Z^2]} \quad (0)$$

so that:

$$C_{point}(R,\theta,Z)=C_{point,0}(R,Z)\cdot[(R_w-R)^2+Z^2]\frac{\sum_i a_i\cos[(i-1)\theta]}{¿¿} \quad (0)$$

or:

$$C_{point}(R,\theta,Z)\cdot¿$$
$$¿\,C_{point,0}(R,Z)\cdot[(R_w-R)^2+Z^2]\sum_i a_i\cos[(i-1)\theta] \quad (0)$$

The coefficients a_i are then derived (up to i=20) for each ring from best fits to the experimental data multiplied by the square of the distance from the scattering centre and symmetrised with respect to $\theta=0$ (fig.8).

Similarly, the fission chamber response to a uniform ring source can be approximated by:

$$C_{ring}(R,Z)=C_{point,0}(R,Z)\cdot\frac{[(R_w-R)^2+Z^2]}{2\pi R}\int_{-\pi}^{\pi} Rd\theta\frac{\sum_i a_i\cos[(i-1)\theta]}{¿¿}¿ \quad (0)$$

Using:

$$\int_0^{\pi}\frac{\cos nx}{1-\alpha\cos x}dx=\frac{\pi}{\sqrt{(1-\alpha^2)}}\left(\frac{1-\sqrt{(1-\alpha^2)}}{\alpha}\right)^n \quad (0)$$

one has an analytic formula for the ring averages:

$$C_{ring}(R,Z)=C_{point,0}(R,Z)\cdot\frac{[(R_w-R)^2+Z^2]}{R\cdot\left[R_w^2+R^2+Z^2\right]}\frac{1}{\sqrt{(1-\alpha^2)}}\sum_i a_i\left(\frac{1-\sqrt{(1-\alpha^2)}}{\alpha}\right)^{i-1} \quad (0)$$

with

$$\alpha=\frac{2R_wR}{\left[R_w^2+R^2+Z^2\right]} \quad (0)$$

With the high-quality ring data obtained in this calibration, it was found that a simple, trapezoidal integral produced the same value as this cosine series fit. When there is sufficient ring data, the simplest evaluation of the calibration factor is by interpolation with:

$$K^{-1}=\frac{\iint RdRdZ\,S_{plasma}(R,Z)\cdot C_{ring}(R,Z)}{\iint RdRdZ\,S_{plasma}(R,Z)} \quad (0)$$

Here, following [2], the radial interpolation is done in two parts. First, the residual variation of $C_{point}\cdot X^2$ is determined by fitting to the radial scan data (fig.7(left)):

$$C_{point,0}(R,Z_0)\cdot\left[(R_w-R)^2+Z_0^2\right]=\left[4.5-\left\{\left(\frac{4.5-2.932}{420-300}\right)^2\left[(420-300)^2-(R-300)^2\right]\right\}^{1/2}\right]\cdot 10^5 \quad (0)$$

A linear fit is then done to the normalised inner, central and outer ring-averaged data:

$$C_{ring}(R,Z_0)/\left(C_{point,0}(R,Z_0)\cdot\left[(R_w-R)^2+Z_0^2\right]\right)=5.6\times10^{-18}R+6.5967\times10^{-15} \qquad (0)$$

The product of the two fits gives the required radial variation, $C_{ring}(R,Z_0)$.

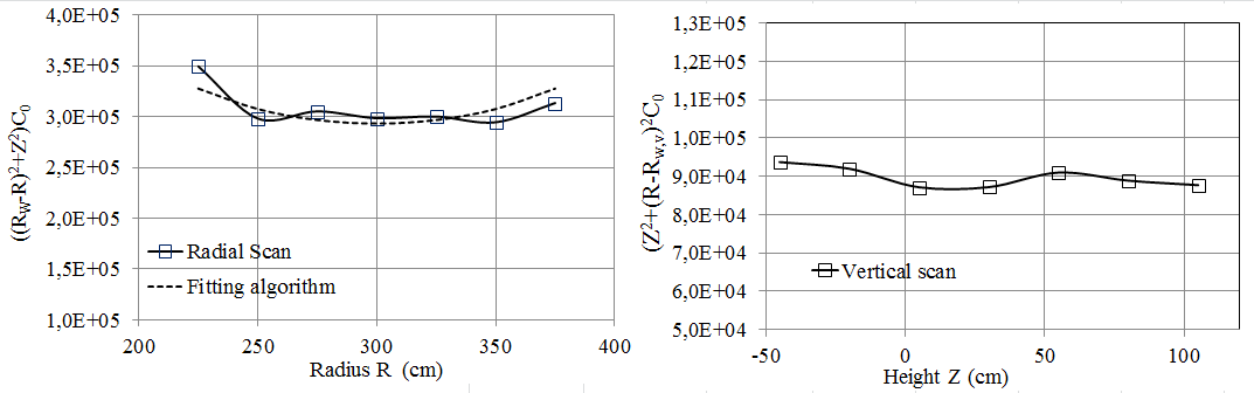

Fig. 7 (Left) Octant 8 radial scan data, multiplied by the square of the distance to the scattering centre with R_w=618 cm. Dashed lines are derived from the fitting algorithm described in the text.
(Right) Octant 8 vertical scan data multiplied by the square of the distance to the scattering centre with $R_{w,v}$=470 cm.

The vertical variation is deduced from the observation that $C_{point}\cdot X^2$ remains approximately constant over the vertical point scan (at $R=300\,cm$ and for $R_{w,v}=470\,cm$ and $Z_0=30\,cm$). This is assumed to be true also for the rings and at all R:

$$C_{ring}(R,Z)=C_{ring}(R,Z_0)\frac{(R_{w,v}-R)^2+Z_0^2}{(R_{w,v}-R)^2+Z^2} \qquad (0)$$

The ring response function, $C_{ring}(R,Z)$, function derived with the analytical procedure is shown in Fig.9. It may be expected that $C_{ring}(R,Z)$ is less accurate outside the region where experimental scan were collected (225 cm < R <375 cm , -45 cm < Z < 105 cm). However, the use of the derived function outside this region is justified by the fact that the neutron source is mostly concentrated in the plasma centre and thus the impact of extrapolating the calibration factor on the derived total neutron rate will be small.

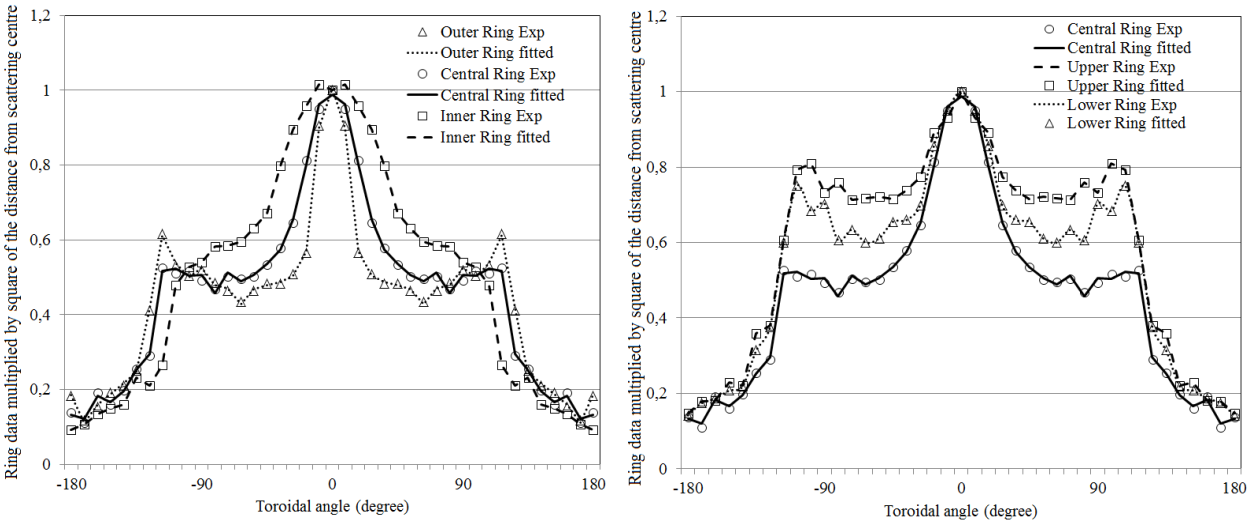

Fig. 8 Ring experimental data for D_1 in Octant 8 multiplied by the square of the distance from the scattering port and symmetrised with respect to the peak, and best fits for (Left) central, outer and inner rings, and for (Right) central, upper and lower rings.

The predictions of the fitting formula for the ring values are given in Table 2:

Table 2 *Measured and fitted response of fission chamber D1 to the Basket Scans, normalised to a unit neutron source.*

	Central Ring	Upper Ring	Lower Ring	Inner Ring	Outer Ring
R	300	300	300	250	350
Z	30	80	-20	30	30
Measured	2.43E-09	2.19E-09	2.37E-09	2.43E-09	2.51E-09
Fitted	2.43E-09	2.30E-09	2.44E-09	2.46E-09	2.63E-09

If the measured C_{ring} decreases, on average, as one moves away from the plasma centre, one would expect the volume source to have a higher effective calibration factor K than that for the central ring and vice versa.

The ring response function has been finally convoluted with a plasma neutron source profile in the form

to derive the effective calibration factor, K, for detector D_1 as a function of neutron emission profile peaking factor γ (solid curve in Fig.10).

It is also possible to derive effective calibration factors by direct interpolation of the ring data on R and Z (dot-dashed curve in Fig.10). The dashed line in Fig.10 is the inverse of the central ring response function and corresponds to infinite peaking. The interpolation method has the advantage that it uses the more relevant ring data more completely and directly than the fitting method. It is, on the other hand, subject to uncertainty when extrapolated outside the measurement range (in the interpolation, the ring response function is held constant when extrapolating). The fitting method provides underlying understanding of the primary path of neutron transport from source to detector as well as detailed contact to the 1980s calibrations. Combining radial and vertical scans in front of the relevant

ports with ring data also permits more efficient access to a wider measurement range than would be required to repeat entire ring measurements.

The analysis shows that the calibration factor is a weak function of the neutron emission profile and differs by less than ~3% from the inverse of the integral of the central ring $F_c = 1/C_{ring}(R=300,Z=30)$ for values of the peaking factor $\gamma>1$. It should be stressed that this analysis is carried out for a neutron source with ^{252}Cf energy spectrum. The result of this simple analysis, which is not used to derive the final calibration factor, has been confirmed by Monte Carlo neutron transport calculations by MCNP code (see Table 3 and the discussion in the next section).

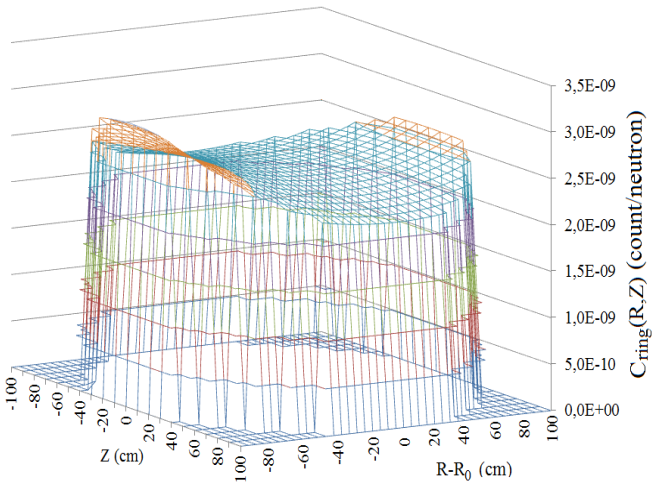

Fig. 9 $C_{ring}(R,Z)$ function as derived from analysis of basket and port scans for D1/Oct 8 detector(fitting approach)

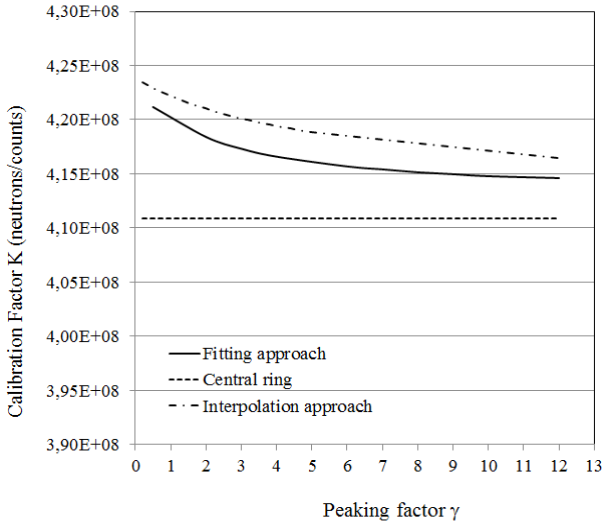

Fig.10 D1/Oct 8 detector calibration factor K as a function of neutron emission profile peaking factor γ

4 Neutronics analyses

Full neutronics analyses [8-12] have been performed to analyse the FCs response functions using the MCNP Monte Carlo particle transport code and a complete model of the JET torus, its torus hall and the major diagnostics therein [13]. This model can also allow for calculation of the corrections due to extraneous effects like the presence of the MASCOT and boom (as shown earlier by the preliminary calculations of Snoj et al [9]). The neutronic properties of the neutron source and the analyses of the neutronic pathways were also investigated in preliminary calculations [10,11] prior to the full examination of the calibration experiment.

For these neutronics analyses a detailed and updated MCNP model of the JET tokamak was used. The geometry of the detailed model is presented in Figure 11. This model includes various items such as antennae and limiters inside as well as the divertor at the bottom of the vacuum vessel. Outside the vessel large structures in the torus hall such as transformer limbs, neutron shield are also present. However, a
large mass of cables, diagnostics, pipes and other materials present in the torus hall are not included in the

model. They are simulated by the addition of a layer of material outside the vessel (visible as orange in Fig. 11, right) the density of which is adjusted so that the calculated fission chamber response best matches the observed response. Once a reasonable match was achieved, the effect of correction factors for energy spectrum, point source to volume source and boom presence could be estimated. In fact, MCNP calculations are only used to calculate corrections to be applied to the experimental data from the central ring.

Modelling of the JET remote handling system is thoroughly described in [9] and [14]. Hence only a brief summary is given here. Any configuration of the JET RH system is defined by 21 coordinates, 9 defining one translation and eight rotations of the boom sections, and 12 defining the rotations of the joints (6 for each of the two arms). Simple shapes, such as boxes and cylinders were used to explicitly model the casing of the RH system components which contain most of the mass (Fig. 12). The interior however, was modelled as a homogenous mixture of materials, such as Al, Fe and Cu, representing the electro-motors, stainless steel presenting wires, cables, W for balance weights, etc. A script was written to prepare MCNP model (input) for every source point, each featuring a different arrangement of the JET RH system components. The model of the JET RH system was then introduced into the full scope model of the JET tokamak as shown in Figure 11.

The calculated correction factors assessing the effect of the RH system on the detector response for individual source positions are presented in Fig.13 (Right). In some positions the corrections are substantial, up to 85%. However, due to the low detector response at those positions, the global corrections for ring integrals are lower, ranging from 2% to 15% (Correction (NO RH)/(RH) in Table 3).

MCNP analyses were also carried out to analyse the overlap data shown in Fig. 6: the calculated ratios of overlap data over central ring data, shown in Fig.14, can reproduce satisfactorily well the measured data for all detectors.

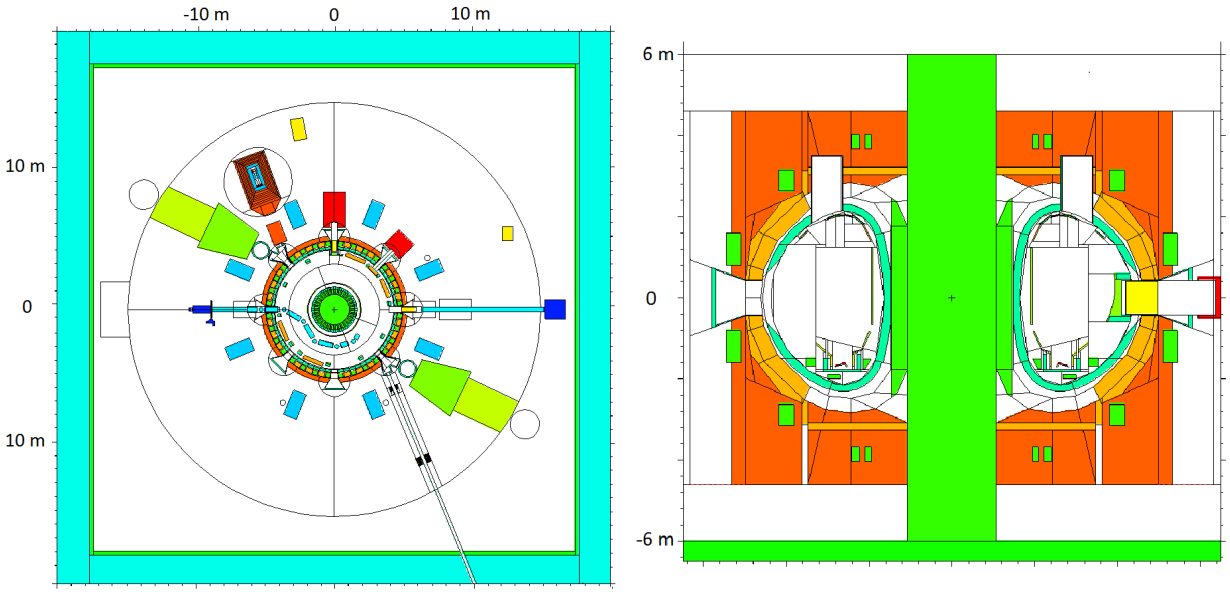

Fig. 11. Horizontal (left) and vertical (right) cross sections of the detailed MCNP model of JET.

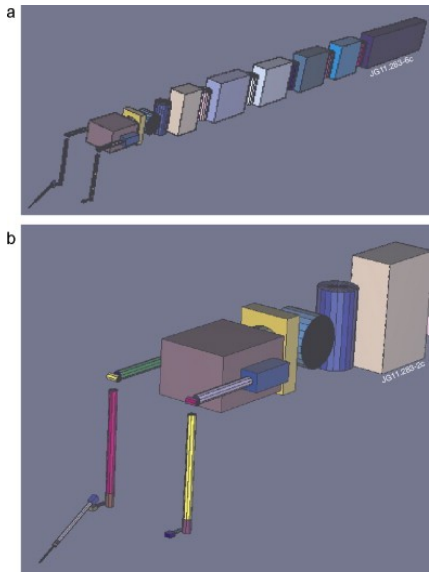

Figure 12. 3D view of the MCNP model of Octant 5 Boom and Mascot in its basic configuration. The colour of the structures does not indicate anything, it is just a colouring system used in MCNP Visual Editor.

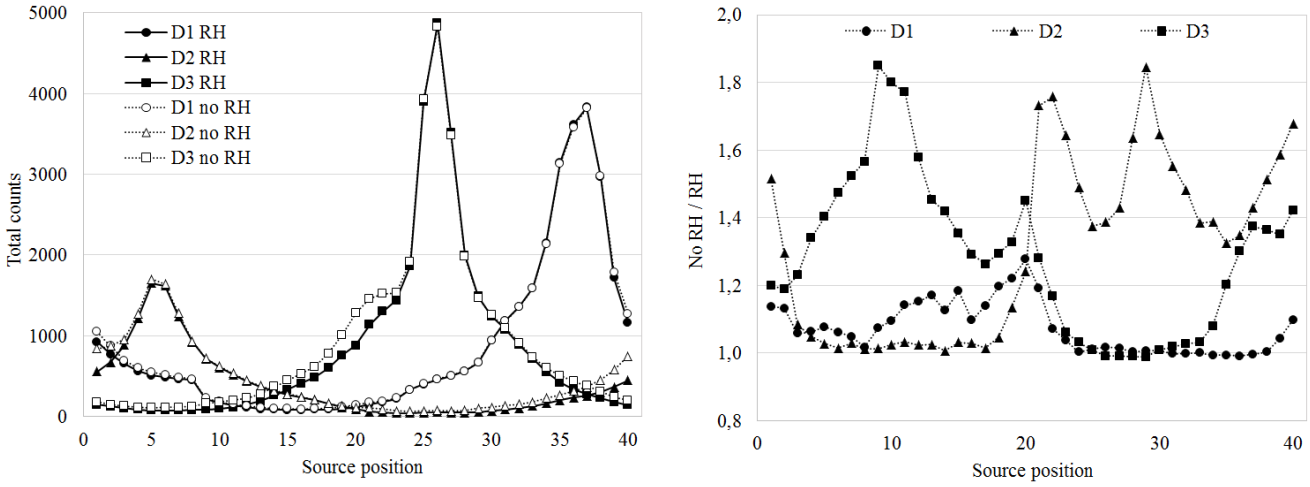

Fig. 13. Left: Calculated detector response with the presence of the RH boom and removing the presence of the RH boom. Right: Correction factors applied to individual measurements (no RH / RH) to remove the effect of the presence of the RH boom

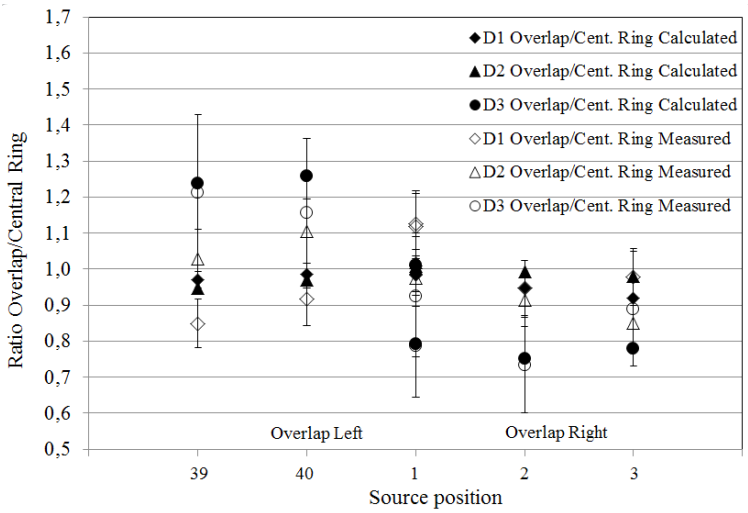

Fig. 14. Measured and calculated ratios of overlap data over central ring data. The error bars represent the statistical uncertainty in the measurements. Statistical errors in MCNP calculations (not shown) are ≤~2%.

Additional corrections were applied to correct for the differences in the neutron emission spectra (Correction DD Ring / Cf Ring, Table 3) and the shape of the source (Correction DD plasma / DD Ring, Table 3). The plasma source used was constructed from 340 toroidal rings each with a square cross section of 10x10 cm. The emissivity assigned to each ring corresponds to a H-mode plasma emissivity with centre at R=310, Z=30 cm.

The corrections due to the differences between the spectra of the calibration neutron source (^{252}Cf) and the DD neutron source are significant due to the differences in the neutron emission spectra and consequently different transparency of the reactor to the emitted neutrons. The correction due to the shape of the neutron source, on the other hand, is below -3% indicating the suitability of the selected ring neutron source used in the calibration and confirming that the corrections for the volume source are small. The sign of the correction, however, is opposite to the one obtained in the analyses described in section 3 and is only in part explained by the shift of the plasma axis to R=310 cm, indicating that the MCNP modelling uncertainties are comparable or larger than the correction itself.

The uncertainty on the measured central ring data are very low (~1%). The statistical uncertainty on the MCNP calculations is also very small (~1%). However, systematic errors in the simulations, due to approximations in the modelling of ports and of surrounding objects, are difficult to estimate. In JET, the activation system is the reference system providing the absolute calibration for neutron yield measurements, due to its almost total insensitivity to changes in the machine external layout. In 2013 the absolute calibration of the activation system was obtained within a total uncertainty of ±9%. The calibration factors obtained independently for the three FCs and the activation system were cross-checked with DD plasmas after the calibration: the neutron yields from DD plasmas measured during the C32a-C33 campaigns in June – August 2014 by the three FCs and the activation system agreed within ±3 %, i.e. well within the combined uncertainty of the four different systems (see Fig.15).

Table 3 *Summary of calculated (MCNP) correction factors for the KN1 FC calibration factors*

	D1 / Oct 8	D2 / Oct 2	D3 / Oct 6
Integral of Central Ring (n/count) measured	4.108 $\cdot 10^8$	7.132 $\cdot 10^8$	3.588 $\cdot 10^8$
Correction (NO RH)/(RH)	1.02	1.15	1.10
Correction DD Ring / Cf Ring	1.14	1.18	1.12
Correction DD plasma / DD Ring	0.973	0.999	0.988
TOTAL Correction Factor	1.131	1.356	1.217
KN1 DD plasma calibration coefficients (n/count)	3.631 $\cdot 10^8$	5.261 $\cdot 10^8$	2.948 $\cdot 10^8$

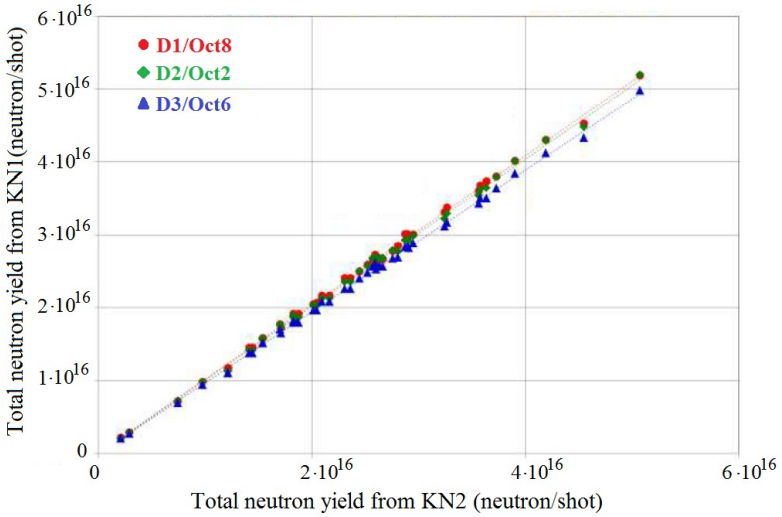

Fig. 15.Comparison of neutron yields per shot as measured from DD plasmas during the C32a-C33 campaigns in June – August 2014 by the three FCs (KN1) and the activation system (KN2).

5 Conclusions

The experimental data obtained in the 2013 neutron calibration of JET fission chambers (KN1) were presented. The integrals of the central ring data were very accurate and reproducible, in spite of the uncertainty on the neutron source positioning. Moving from the central to the non-central rings (50 cm apart) caused a maximum change in the integral responses of fission chambers of about 11% mainly due to the varying collimating effect of the vessel main horizontal ports.

The experimental data were first analysed following an analytical approach adopted in the previous neutron calibrations at JET. In particular, the ring and the radial and vertical scan data were used to derive a calibration function for the volumetric plasma source to understand the importance of the different plasma regions and of different spatial profiles of neutron emissivity on KN1 response. The main finding of this approach is that the volume calibration function is very close to the calibration function obtained with the source on the central ring, within 3% for peaking factors of the plasma neutron emissivity profile

larger than 1. This finding has been confirmed by neutronics analyses. Neutron calibrations can therefore be performed accurately with neutron source data on the central ring only.

Neutronics analyses have also been performed to calculate the correction factors needed to derive the plasma calibration factors taking into account the different energy spectrum and angular emission distribution of the calibrating (point) ^{252}Cf source, the discrete positions compared to the plasma volumetric source, and the calibration circumstances characterised by the presence of the RH boom. DD neutrons produce a higher response than ^{252}Cf neutrons by 12-18%. This is partly due to the intrinsic response function of fission chambers, which has a maximum at about 1-2 MeV, and partly to the fact that the DD neutrons are more penetrating than ^{252}Cf neutrons. The corrections due to the presence of the RH boom amount to 2%-15% depending on the detector position.

After the calibration, the neutron yields from DD plasmas measured by the three FCs and the activation system agreed within ±3%.

Acknowledgements:

This work has been carried out partly within the European Fusion Development Agreement (EFDA) and partly within the framework of the EUROfusion Consortium and has received funding from the Euratom research and training programme 2014-2018 under grant agreement No 633053. The views and opinions expressed herein do not necessarily reflect those of the European Commission.

References

[1]. B.J. Laundy and O.N. Jarvis, "Numerical study of the calibration factors for the neutron counters in use at the Joint European torus", Fusion Technology, **24**, 1993, pp. 150 (also JET-P(92)60).

[2]. O.N. Jarvis, J. Kallne, G. Sadler, P. van Belle, M. Hone, V. Merlo, E. W. Lees, M.T. Swinhoe, A.R. Talbot and B. H. Armitage, "Further calibrations of the time-resolved neutron yield monitor (KN1)", JET Internal Report JET-IR(85)06, 1986.

[3]. O.N. Jarvis, G. Sadler, P. van Bell and T. Elevant: "In-vessel calibration of the JET neutron monitors using a 252Cf neutron source: Difficulties experienced", Review of Scientific Instruments, **61**(10), 1990, pp. 3172-3174.

[4]. O.N. Jarvis, E. Clipsham, M. Hone, B. Laundy, M. Pillon, M. Rapisarda, G. Sadler, P. van Belle and K.A.Verschuur, "Use of activation techniques at JET for the measurement of neutron yields from deuterium plasmas", Fusion Technology, **20**, 1991, pp. 265-284 (and JET-P(90) 46)

[5] G. F. Matthews, M. Beurskens, S. Brezinsek, M. Groth, E. Joffrin, A. Loving, M. Kear, M-L. Mayoral, R. Neu, P. Prior et al., JET ITER-like wall—overview and experimental programme, Physica Scripta, Volume 2011, T145 (2011)

[6] D.B. Syme et al., Fusion yield measurements on JET and their calibration, Fus. Eng. Design, Volume 89, 2014, pp 2766-2775

[7] P. Batistoni et al., Technological exploitation of Deuterium–Tritium operations at JET in support of ITER design, operation and safety, Fus. Eng. Design, Volumes 109–111, 2016, pp 278-285

[8] D.B. Syme et al., Fusion yield measurements on JET and their calibration, Nuc. Eng. Design,

Volume 246, 2012, pp 185–190

[9] L. Snoj, I. Lengar, A. Čufar, B. Syme, S. Popovichev, S. Conroy, L. Meredith, Calculations to support JET neutron yield calibration: Modelling of the JET remote handling system, Nuclear Engineering and Design, **261**, 2013, pp. 244-250.

[10] L. Snoj, A. Trkov, I. Lengar, S. Popovichev, S. Conroy, B. Syme, Calculations to support JET neutron yield calibration: Neutron scattering in source holder, Fusion Engineering and Design, **87**, 2012, pp. 1846-1852.

[11] L. Snoj, B. Syme, S. Popovichev, I. Lengar, S. Conroy, Calculations to support JET neutron yield calibration: Contributions to the external neutron monitor responses, Nuclear Engineering and Design, **246**, 2012, pp. 191-197.

[12] L. Snoj et al., Neutronic analysis of JET external neutron monitor response, Fusion Engineering and Design Volumes 109–111, 2016, pp. 99–103

[13] M. Gatu-Johnson et al., Modeling and TOFOR measurements of scattered neutrons at JET, Plasma Physics and Controlled Fusion, **52**, vol 8 (2010)

[14] L. Snoj, I. Lengar, A. Čufar, B. Syme, S. Popovichev, S. Conroy, L. Meredith, Modelling of the remote handling systems with MCNP - JET fusion reactor example case. V: Joint International conference on mathematics and computation (M&C), supercomputing in nuclear applications (SNA) and the Monte Carlo (MC) method, Joint International Conference on Mathematics and Computation (M&C), Supercomputing in Nuclear Applications (SNA) and the Monte Carlo (MC) Method, 19-23 April 2015, Nashville, 2015